J Biomol NMR (2014) 58:37–47
DOI 10.1007/s10858-013-9802-2

ARTICLE

High-resolution paramagnetically enhanced solid-state NMR spectroscopy of membrane proteins at fast magic angle spinning

Meaghan E. Ward · Shenlin Wang · Sridevi Krishnamurthy · Howard Hutchins · Michael Fey · Leonid S. Brown · Vladimir Ladizhansky

Received: 24 October 2013 / Accepted: 6 December 2013 / Published online: 13 December 2013

Abstract Magic angle spinning nuclear magnetic resonance (MAS NMR) is well suited for the study of membrane proteins in membrane mimetic and native membrane environments. These experiments often suffer from low sensitivity, due in part to the long recycle delays required for magnetization and probe recovery, as well as detection of low gamma nuclei. In ultrafast MAS experiments sensitivity can be enhanced through the use of low power sequences combined with paramagnetically enhanced relaxation times to reduce recycle delays, as well as proton detected experiments. In this work we investigate the sensitivity of ^{13}C and ^{1}H detected experiments applied to 27 kDa membrane proteins reconstituted in lipids and packed in small 1.3 mm MAS NMR rotors. We demonstrate that spin diffusion is sufficient to uniformly distribute paramagnetic relaxation enhancement provided by either covalently bound or dissolved CuEDTA over 7TM alpha helical membrane proteins. Using paramagnetic enhancement and low power decoupling in carbon detected experiments we can recycle experiments $\sim$13 times faster than under traditional conditions. However, due to the small sample volume the overall sensitivity per unit time is still lower than that seen in the 3.2 mm probe. Proton detected experiments, however, showed increased efficiency and it was found that the 1.3 mm probe could achieve sensitivity comparable to that of the 3.2 mm in a given amount of time. This is an attractive prospect for samples of limited quantity, as this allows for a reduction in the amount of protein that needs to be produced without the necessity for increased experimental time.

Keywords Magic angle spinning · Solid-state NMR · Paramagnetic relaxation enhancement · Proton detection · Membrane proteins · Condensed data collection

M. E. Ward · S. Wang · L. S. Brown · V. Ladizhansky (✉)
Department of Physics and Biophysics Interdepartmental Group, University of Guelph, Guelph, ON, Canada
e-mail: vladizha@uoguelph.ca

Present Address:
S. Wang
Beijing NMR Center, Peking University, Beijing, China

S. Krishnamurthy · H. Hutchins · M. Fey
Bruker Biospin, Billerica, MA 01821, USA

Introduction

Solid-state NMR (SSNMR) spectroscopy is emerging as a powerful method for the study of membrane protein structure and dynamics, and has already provided a wealth of information on many biologically important systems (Cady et al. 2010; Hong 2007; Hu et al. 2010; McDermott 2009; Naito 2009; Park et al. 2012; Ramamoorthy 2009; Renault et al. 2010; Shahid et al. 2012; Sharma et al. 2010; Wang et al. 2013). Typically, SSNMR studies require milligram quantities of sample and employ moderate spinning frequencies (10–20 kHz) and high radio-frequency (RF) power decoupling. Such experimental conditions require long recycle delays between successive scans (1.7 s or longer) for the recovery of spin polarization and to avoid probe and sample damage caused by the application of high power RF.

It has recently been demonstrated that recycle delay requirements can be reduced under fast MAS conditions, as the application of fast spinning frequencies (40 kHz or higher) averages anisotropic interactions more efficiently, eliminating the need for high power decoupling (Ernst et al. 2004; Kotecha et al. 2007; Vijayan et al. 2009). When

entirely low-power schemes are combined with the introduction of paramagnetic dopant to reduce proton relaxation times, recycle delays can be reduced by an order of magnitude (Wickramasinghe et al. 2007). Such paramagnetic dopants cause rapid spin–lattice relaxation of nearby protons while rapid interproton spin diffusion redistributes the paramagnetic relaxation enhancement effect throughout the sample. Recently, Ishii and co-workers used fast MAS (40 kHz), low power decoupling, and short recycle delays enabled by exogenously added Cu(II)-EDTA as a paramagnetic relaxation agent to develop the paramagnetic relaxation-assisted condensed data collection (PACC) scheme (Wickramasinghe et al. 2009). They have demonstrated that the PACC scheme enables SSNMR studies of small, nanomolar amounts of ^{13}C,^{15}N-labeled biomolecules.

The PACC scheme has further been extended to systems containing covalently attached paramagnetic tags. The Jaroniec lab has demonstrated similar spin–lattice relaxation time reduction in microcrystalline GB1 (the first immunoglobulin binding domain of protein G), using EDTA tags loaded with Cu(II) (CuEDTA) covalently attached to cysteine residues introduced by site directed mutagenesis (Nadaud et al. 2010). An additional benefit of the covalent introduction of Cu(II) is that it allows for quantification of PREs through the ^{15}N spin–lattice relaxation rates, T_1, which can be used to extract distance restraints for protein structure determination (Sengupta et al. 2012). The effects of paramagnetic relaxation enhancement and the performance of the PACC scheme were recently investigated in membrane proteins. Ramamoorthy and co-workers and Rienstra and co-workers have demonstrated that copper-chelated lipids and CuEDTA added to the buffer can be used to speed up SSNMR data acquisition in membrane proteins (Yamamoto et al. 2010; Tang et al. 2011). The latter study, which was performed on the transmembrane protein DsbB, employed 1.6 mm rotors and spinning frequencies of 36 kHz. Although very short proton T_1 values of 50–80 ms were obtained, relatively long recycle delays of 0.3–0.5 s were still necessary to avoid sample damage and to minimize probe heating effects.

Recent advances in probe design have extended the range of spinning frequencies up to $\sim$80 kHz (Nishiyama et al. 2011). Fast spinning frequencies enable the use of low-power decoupling (Ernst et al. 2004; Kotecha et al. 2007; Vijayan et al. 2009), facilitate proton detected experiments (Lewandowski et al. 2011; Marchetti et al. 2012; Zhou et al. 2007), and suppress coherent contributions to relaxation rates, thus providing direct access to dynamic information (Lewandowski et al. 2010; Schanda et al. 2010). Due to the use of small rotors, which have a higher sensitivity per unit sample, ultrafast MAS probes are an attractive option for the study of proteins that can only be produced in small quantities, particularly eukaryotic membrane proteins (Egorova-Zachernyuk et al. 2010, 2011; Werner et al. 2008). However, an important challenge in the use of these rotors is the drastically reduced sensitivity caused by the decrease in sample volume. For example, when experiments using 1.3 and 3.2 mm rotors are compared the volume ratio contributes a factor of $\sim$15 or more to the relative sensitivity. Therefore, it is important to investigate the extent to which the benefits offered by ultrafast MAS, such as the increased coil efficiency, accelerated acquisition schemes, and the potential for proton detection, can compensate for this drastic reduction in the sample volume.

In this work we investigate the performance of the PACC scheme when applied to larger, 27 kDa membrane proteins reconstituted in lipids and packed in small 1.3 mm MAS NMR rotors. We examine the sensitivity of ^{13}C-detected experiments using a lipid-reconstituted seven transmembrane (7TM) α-helical protein, *Anabaena* Sensory Rhodopsin (ASR) (Jung et al. 2003). ASR forms stable trimers in the lipid environment (Wang et al. 2012, 2013) and gives well-resolved, high signal-to-noise ratio spectra with typical carbon and nitrogen line widths of 0.5 ppm (Shi et al. 2011). We evaluate two different ways of introducing paramagnetic dopants, through the addition of CuEDTA into the buffer and by covalently attaching CuEDTA to a cysteine introduced by mutagenesis.

In contrast to previous studies on GB1 (Nadaud et al. 2010), we find that in the larger, 27 kDa ASR the single covalently attached CuEDTA leads to only a small overall decrease in proton spin–lattice relaxation times. On the other hand, we found that CuEDTA added to the buffer results in significant and fairly uniform shortening of ^{1}H T_1 relaxation in ASR samples, increasing in effectiveness as the CuEDTA concentration increases. Overall, although we observe a significant increase in the signal-to-noise ratio per unit sample, we conclude that even with extensive paramagnetic doping and fast experimental recycling, data collection for ^{13}C-detected experiments with the 1.3 mm probe is ultimately much less efficient than with the 3.2 mm probe.

We further investigate the effects of fast MAS and paramagnetic doping on proton detection experiments on a fully deuterated 7TM protein, proteorhodopsin (PR), which is similar to ASR in terms of its stability and the obtained spectral quality (Shi et al. 2009a, b). For proton-detected experiments the sensitivity per unit time of the 1.3 mm probe is found to be comparable to that of the 3.2 mm probe, which allows for experiments of similar sensitivity to be performed on a drastically reduced sample quantity, in agreement with previous observations on the α-spectrin SH3 domain when the RAP (Reduced Adjoining Protonation) labeling scheme was utilized (Asami et al. 2012).

Experimental section

Materials

Common chemicals of reagent grade were purchased from either Fisher Scientific (Unionville, Ontario, Canada) or Sigma-Aldrich (Oakville, Ontario, Canada). Isotopically labeled compounds, such as $^{15}NH_4Cl$ and $^{13}C_6$–glucose were obtained from Cambridge Isotope Laboratories (Andover, MA). The Ni^{2+}-NTA (nitrilotriacetic acid) agarose resin was purchased from Qiagen (Mississauga, Ontario, Canada). Lipids were purchased from Avanti Polar Lipids (Alabaster, AL).

Expression and purification

Synthesis of uniformly ^{13}C, ^{15}N labeled N148C mutant of Anabaena sensory rhodopsin

[U-^{13}C,^{15}N]–labeled, C-terminally truncated, His-tagged, N148C mutant ASR (UCN N148C ASR) was produced according to a protocol published for wild-type (WT) ASR (Shi et al. 2011). Protein was expressed in BL21-Codon-plus-RIL *E. coli* grown on M9 minimal medium at 30 °C, using 4 g of [U-^{13}C] labeled glucose and 1 g of $^{15}NH_4Cl$ per litre of culture as the sole carbon and nitrogen sources. When the culture reached a target cell density of $A_{600} = 0.4$ OD protein expression was induced by the addition of IPTG to a concentration of 1 mM and retinal to a final concentration of 7.5 μM. After ~21 h the cells were collected by centrifugation, pre-treated with lysozyme (12 mg/l of culture) and DNase I (600 units per litre of culture) and then broken by sonication. The membrane fraction was then solubilized in 1 % DDM (n-dodecyl β-d-maltoside) at 4 °C, and purified following the batch procedure described in the Qiagen Ni^{2+}-NTA resin manual. Approximately 7 mg of UCN N148C ASR was purified from 1 l of culture. The molar amount of ASR was determined by the absorbance of opsin-bound retinal, using the extinction coefficient of 48,000 $M^{-1}cm^{-1}$ (Wada et al. 2008). Purified proteins were buffer-exchanged using an Amicon Ultra-15 10 K centrifugal filter (Millipore, Massachusetts, MA, USA) into pH 8.0 buffer (5 mM Tris, 10 mM NaCl, 0.05 % DDM), and concentrated to ~1 mg/ml (36 μM).

Synthesis of uniformly ^{2}H, ^{13}C, ^{15}N labeled proteorhodopsin

[U-^{13}C,^{15}N,^{2}H]- PR (UCND PR) samples were produced as described previously (Ward et al. 2011). The procedure for producing and purifying this protein is the same as that described above for ASR, with the following key differences. First, the cells were grown using [U-^{2}H,^{13}C]-labeled glucose (4 g) as the sole carbon source and with D_2O (99.9 % purity) in the expression media. The cells were grown to a high cell density in 2 ml (24 h) and then 25 ml (15 h) volumes before being added to the 1 l culture to create a target cell density of $A_{600} = 0.1$ OD. After induction with IPTG, retinal was added at intervals of ~7 h to a final concentration of 7.5 μM. PR solubilization was performed using 1 % Triton X-100, which was exchanged for DDM on the resin during purification. Approximately 15 mg of UCND PR was purified from 1 l of culture. The molar amount of PR was determined by the absorbance of opsin-bound retinal, using the extinction coefficient of 44,000 $M^{-1}cm^{-1}$ (Friedrich et al. 2002).

Incorporation of paramagnetic labels and lipid reconstitution

To investigate the PRE effect on our membrane proteins, four samples of uniformly labeled N148C ASR were created: (1) a control sample without copper (ASR), (2) a sample with CuEDTA covalently attached to C148 (ASRCu), and samples with (3) 40 mM (ASR40Cu), and (4) 80 mM CuEDTA (ASR80Cu) in the solvent (summarized in Table 1). The latter three samples are estimated to contain approximately 1, 4 and 8 paramagnetic centers per protein, respectively. The number of CuEDTA molecules per protein was estimated using the relative intensities of the water and lipid peaks in a 1D proton detected spectra. Given these relative intensities and the known protein to lipid ratio, the volume of water available per protein molecule can be calculated, and thus the number of CuEDTA molecules in that volume of water for a given concentration can be determined.

It has been previously shown that the native cysteine residues present in ASR (at positions 134, 137, and 203) are not accessible for reaction, as these residues are buried in the intermembrane region (Wang et al. 2012). Thus, non-native, solvent-accessible cysteines introduced into the wild-type background of ASR can be selectively labeled through the addition of cysteine-specific paramagnetic tags. N148 was chosen as a mutation site as it is located on the E–F loop and therefore should be accessible for binding and lead to good dispersion of the paramagnetic labels throughout the trimer. Furthermore, expression of N148C ASR has been found to be more efficient than that of WT ASR and other cysteine mutants, such as S26C, which we have examined (Wang et al. 2012).

To test the accessibility of C148 to paramagnetic labeling, a sample of solubilized N148C ASR was incubated for 1 h at room temperature with a 20-fold molar excess of [S-Methanethiosulfonylcysteaminyl] ethylenediamine-N,N,N′,N′-Tetraacetic Acid (MTS-EDTA, purchased from Toronto Research

Table 1 Sample preparation conditions and bulk ^{1}H T_1 Values of N148C ASR and PR samples under 50 kHz MAS

Sample	ASR	ASRCu	ASR40Cu	ASR80Cu	DPR	DPR80Cu
Preparation Conditions	ASR with MTS-EDTA bound to C148	UCN N148C ASR with MTS-CuEDTA bound to C148	UCN N148C ASR with MMTS bound to C148 with 40 mM CuEDTA in the solvent	UCN N148C ASR with MMTS bound to C148 with 80 mM CuEDTA in the solvent	UCND PR	UCNDPR with 80 mM CuEDTA in the solvent
Bulk ^{1}H T_1 (ms)	340 ± 6	227 ± 10	113 ± 4	105 ± 5	460 ± 20	189 ± 16

Chemicals Inc., Ontario, Canada). Unreacted reagent was removed by buffer-exchange. The completeness of spin labeling was monitored and confirmed by Matrix Assisted Laser Desorption Ionization Mass Spectroscopy (MALDI-MS). Direct comparisons of solid-state NMR spectra between WT ASR and the N148C mutant reveals that the mutant retains essentially the same fold as the wild-type, with only a few perturbations to line widths and chemical shifts being observed in residues located close to the mutation site. For consistency, all ASR samples were prepared using N148C ASR.

The covalently CuEDTA-labeled protein (ASRCu in the following) was then mixed with liposomes, prepared by hydrating dried DMPC and DMPA mixed at a 9:1 ratio (w/w), at a protein:lipid ratio of 2:1 (w/w) and incubated for 6 h at 4 °C before Bio-Beads SM (Bio-Rad Laboratories) were added for detergent removal. The functionality and protein to lipid ratio of the reconstituted protein have been tested using visible and FTIR spectroscopy, as described previously (Shi et al. 2006, 2009a).

ASR samples with CuEDTA incorporated in the buffer (ASR40Cu and ASR80Cu) were prepared by first mixing solubilized protein with a 20-fold molar excess of methyl methanethiosulfonate (MMTS, purchased from Toronto Research Chemicals Inc., Ontario, Canada) (Religa et al. 2011) to block the cysteine SH group. Unreacted reagent was then removed by buffer-exchange and the proteins were reconstituted into liposomes as described previously for ASRCu. After reconstitution, liposomes were resuspended in a large volume of buffer containing the desired concentration of ethylenediaminetetraacetic acid (EDTA), tetrasodium salt, and copper sulfate and incubated for 1 h at 4 °C before being ultra centrifuged for packing. It is important to note that the CuEDTA concentration was calculated excluding the volume of the protein and lipids in the sample, reporting on its amount in the solvent surrounding the proteoliposomes.

For proton detected experiments two samples of UCND PR were made: (1) a control sample without copper (DPR) and (2) a sample with 80 mM CuEDTA in the solvent (DPR80Cu). Reconstitution and CuEDTA incorporation was performed as described above for ASR. After reconstitution, the UCND PR proteoliposomes were incubated in a 40:60 H_2O:D_2O buffer for ~24 h before the addition of CuEDTA and collection by ultra centrifugation.

MAS SSNMR spectroscopy

All NMR experiments were performed on a Bruker Biospin Avance III standard bore spectrometer operating at 800.230 MHz using a 1.3 mm ^{2}H-^{1}H-^{13}C-^{15}N probe used in triple resonance $^{1}H/^{13}C/^{15}N$ mode, with spinning at 50 kHz, and at the effective temperature of ~15 °C in all experiments. Cooling was achieved using nitrogen gas cooled through a liquid nitrogen heat exchanger. The effective sample temperature was calibrated using the temperature dependence of the chemical shift of ^{79}Br in KBr (Thurber and Tycko 2009). Although higher spinning frequencies were achievable, maintaining the sample temperature in the range optimal for sample stability required a much higher flow of cold nitrogen gas, resulting in overcooling of the shims in a standard bore magnet.

For each sample approximately 0.75–1 mg of UCN N148C ASR or UCND PR was center-packed in a 1.3 mm rotor and sealed using silicone plugs. For each of the samples the bulk proton T_1 was measured (discussed in the Results section) and the recycle delay D_1 was adjusted to $1.3T_1$ to maximize the signal to noise ratio in a given time ($(S/N)_T$) as described by Eq. 1:

$$(S/N)_T \propto \left(1 - e^{-D_1/T_1}\right)\sqrt{1/D_1} \quad (1)$$

Here, we account for both the signal loss due to incomplete magnetization recovery, $\left(1 - e^{-D_1/T_1}\right)$, and the signal enhancement due to the increased number of scans, $\left(\sqrt{1/D_1}\right)$. Samples were stable over the course of the NMR experiments, and showed no signs of degradation even in measurements with recycle delays of 100 ms.

In Fig. 1 we show the pulse sequences used to record data. Typical π/2 pulses were 1.6 μs for ^{1}H, 4 μs for ^{13}C, and 5.6 μs for ^{15}N. The $^{1}H/^{15}N$ cross-polarization (CP) (Pines et al. 1973) contact time was 2 ms, with a constant RF field of 30 kHz on nitrogen, while the proton lock field was ramped linearly around the $n = 1$ Hartmann–Hahn

condition (Hartmann and Hahn 1962). $^{15}N/^{13}C_{\alpha}$ band-selective transfers (Baldus et al. 1998) were implemented with a contact time of 5 ms with a constant lock field of 20 kHz strength applied on ^{15}N, while the ^{13}C field was ramped linearly (10 % ramp) around 30 kHz. No proton decoupling was applied during $^{15}N/^{13}C_{\alpha}$ CP. Low power TPPM48 (Kotecha et al. 2007) proton decoupling optimized around 12 kHz was used during ^{15}N and ^{13}C chemical shift evolutions. Proton detected ^{1}H-^{15}N correlation experiments used WALTZ-16 (Shaka et al. 1983) for ^{15}N decoupling during direct acquisition. Water suppression was accomplished by applying a train of pulses at an RF intensity of 25 kHz, and phase shifted by $\pi/2$ every 12 ms for 240 ms.

Chemical shifts were referenced to DSS using the ^{13}C adamantane downfield peak resonating at 40.48 ppm as a secondary external standard (Morcombe and Zilm 2003). Data processing was performed using NMRPipe (Delaglio et al. 1995) or TopSpin 3.1 (Bruker, Karlsruhe, Germany). Noise analysis and peak picking were performed in the CARA (Keller 2004) environment. Estimations of bulk T_1 were done by analyzing the spectral intensity in TopSpin 3.1.

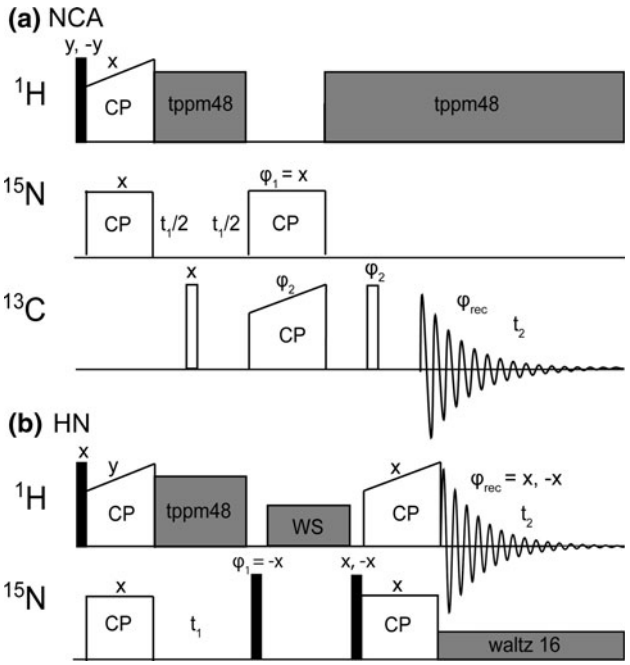

Fig. 1 Pulse sequences for **a** 2D NCA and **b** ^{1}H-detected ^{1}H-^{15}N chemical shift correlation experiments. Filled and hollow bars represent $\pi/2$ and π pulses respectively. In both experiments TPPI (Marion and Wüthrich 1983) phase-sensitive detection is obtained in the indirect t_1 dimension by incrementing φ_1 by 90°. In **a** the following phase cycle is used: $\varphi_2 = (x, x, y, y, -x, -x, -y, -y)$ and $\varphi_{rec} = (x, -x, y, -y, -x, x, -y, y)$. The water suppression period (WS) consisted of a train of pulses with an RF intensity of 25 kHz, phase shifted by $\pi/2$ every 12 ms for 240 ms

Results and discussion

Solvent accessibility

Unlike soluble proteins, membrane embedded ASR and PR have their hydrophobic cores and lateral surfaces protected from solvent. Membrane protein accessibility to polar solutes may be further affected by their orientation in the lipid bilayer. To illustrate this, in Fig. 2a we show a schematic representation of a proteoliposome with the extracellular surface of ASR facing the interior, which could be inaccessible to CuEDTA. Although the morphology of our sample is most likely very different because of the high protein to lipid ratio (approximately 1:20 molar ratio) and low water content, some protein molecules could still be inaccessible to CuEDTA. To study the accessibility of both sides of the proteins to solvent after reconstitution, an unlabeled sample of N148C ASR was reconstituted in the presence of the hydrophilic negatively charged dye 8-hydroxyl-1,3,6-pyrenetrisulfonate (pyranine), which has absorption bands centered at 370, 400, and 460 nm (Kano and Fendler 1978). The proteoliposomes were spun down and then resuspended in a small volume of fresh buffer. Visual inspection of absorption spectra, shown in Fig. 2b, confirmed that the proteoliposomes do not retain pyranine upon buffer exchange, indicating that both sides of the protein are equally accessible to polar solutes.

PRE in N148C ASR ^{13}C-detected experiments

To optimize sample preparation conditions and the parameters of NMR experiments, we first measured the bulk ^{1}H T_1 of ASR, ASRCu, ASR40Cu, and ASR80Cu using an ^{15}N-detected proton saturation recovery experiment (Markley 1971). These samples are estimated to contain 0, 1, 4 and 8 CuEDTA molecules per protein molecule, as described in the Methods section. Measured ^{1}H T_1 values are summarized in Table 1 and discussed in the following.

We observe a relatively short ^{1}H T_1 value of 340 ms for the diamagnetic ASR sample. A similar bulk T_1 value of $\sim$350 ms was measured at a slower spinning frequency of 14.3 kHz, indicating that interproton spin diffusion is not greatly affected by spinning. The observed values fall into the range of values previously reported for other diamagnetic proteins, including ubiquitin (230 ms) (Wickramasinghe et al. 2009), GB1 (450 ms) (Nadaud et al. 2010), DsbB (490 ms) (Tang et al. 2011), and Aβ amyloid fibrils (560 ms) (Wickramasinghe et al. 2009). This variation in T_1 values is likely related to the different states of these proteins (microcrystalline, precipitated, lipid embedded), as well as the different spinning frequencies and temperatures at which experiments were performed.

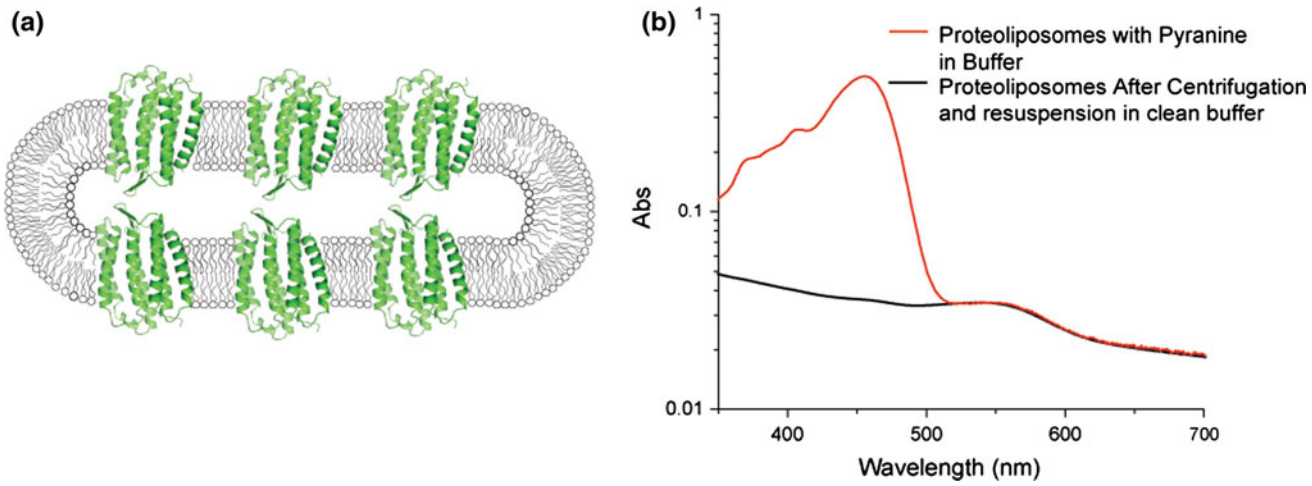

Fig. 2 **a** Schematic representation of lipid reconstituted ASR at a high protein to lipid ratio and low water content, shown to illustrate that sides of the protein may be inaccessible to CuEDTA. Only one of the two possible orientations of the protein in the lipids is shown. **b** Absorption spectra of liposomes containing ASR reconstituted in the presence of 5 mM pyranine immediately following removal of biobeads (*red*) and following pelleting and resuspension in pyranine-free buffer (*black*) at pH 8.0 which shows that pyranine is not retained in the proteoliposomes

In ASRCu, the addition of a single covalently attached tag leads to a moderate decrease in the bulk proton T_1 value from 340 to 227 ms. We note that a much larger bulk proton PRE effect was observed in microcrystalline GB1, with the bulk T_1 being reduced from 450 to 120 ms after the addition of a single covalently attached CuEDTA (Nadaud et al. 2010). As the possibility of incomplete labeling has been ruled out through MALDI-MS, it is likely that the significantly reduced enhancement of the bulk ^{1}H T_1 is due to the much larger size of ASR, as the surface to volume ratio is much smaller in ASR. Additionally, the interproton spin diffusion required to transfer the paramagnetic enhancement throughout the entire protein may also be less efficient. Thus, it appears that a single covalently attached CuEDTA paramagnetic tag is not sufficient to achieve the desirable shortening of the proton spin–lattice relaxation times in our samples.

As we estimate that a single covalently attached CuEDTA is equivalent to $\sim$10 mM of free CuEDTA, it is likely that an increase in CuEDTA concentration would further reduce the bulk ^{1}H T_1. To verify this, we prepared ASR samples with 40 mM and 80 mM CuEDTA in the solvent. Not only are the concentrations of CuEDTA in ASR40Cu and ASR80Cu estimated to be approximately four and eight times higher than that in ASRCu, but the paramagnetic dopants will now have access to both sides of the protein. This allows loops on both sides of the protein to be in contact with the paramagnetic dopant, which likely doubles the effective surface area to volume ratio and reduces the distance which the proton spin polarization must travel. Accordingly, we see a large decrease in the bulk ^{1}H T_1 to 113 ms in ASR40Cu. Further increase in the CuEDTA concentration to 80 mM results in only a marginal decrease of the bulk proton T_1 to 105 ms, which indicates that the spin–lattice relaxation enhancement effect is approaching saturation in this range of concentrations.

To investigate site-specific ^{1}H relaxation enhancement and possible chemical shift and line width perturbations caused by the different paramagnetic labeling schemes, 2D NCA experiments were run on all four samples: ASR, ASRCu, ASR40Cu, and ASR80Cu. All spectra were collected over similar lengths of time ($\sim$13 h), and with recycle delays $D_1 = 1.3T_1$ adjusted according to the measured bulk T_1 values (Table 1). As T_1 values are progressively shortened with increasing levels of paramagnetic doping, one expects that the sensitivity would increase according to the increasing number of scans.

In Fig. 3 we show 2D NCA spectra measured on the four samples with different levels of paramagnetic doping. We expect an average sensitivity increases of $\sim$1.2, 1.55, and 1.6 in ASRCu, ASR40Cu, and ASR80Cu respectively when compared to ASR, based on the number of scans performed in each experiment. The resolution of all four spectra collected under low power decoupling conditions (Kotecha et al. 2007) is comparable to that obtainable in a 3.2 mm Bruker E-free probe (Shi et al. 2011), albeit the absolute sensitivity (i.e., sensitivity from a fully packed rotor) is lower (discussed in the following). The overall structure of the spectra remains the same with the addition of paramagnetic doping, with only a few insignificant perturbations to peak positions being observed. Slight inhomogeneous line broadening, mostly in the indirect ^{15}N dimension, was observed in ASRCu and ASR40Cu. The broadening is uniform over the affected spectra and is not present in the ASR80Cu sample. As Cu(II) mostly enhances longitudinal relaxation rates and has a small

effect on T_2 (Bertini et al. 2001; Jaroniec 2012), the observed broadening is likely due to variations in the reconstitution conditions. We did not observe instances in which a peak appears in the spectrum for the diamagnetic sample but is not present in the paramagnetic samples, indicating that the addition of CuETDA, either covalently bound or in the buffer, does not perturb the structure of ASR or significantly affect sample quality.

Overall, increasing the concentration of CuEDTA results in progressively better sensitivity per unit time. To determine if this enhancement is relatively uniform throughout the protein we performed a site-specific analysis of the signal-to-noise ratio of peaks which were resolved in all four spectra, shown in Fig. 4. We expect that if paramagnetic T_1 enhancement were not transferred uniformly throughout the protein through spin diffusion then we would see a pattern of reduced sensitivity enhancement in residues which are located far from the paramagnetic labels due to the fast recycling and slower magnetization recovery.

In agreement with the bulk T_1 estimates, moderate enhancement with an average value of 1.2 ± 0.2 is observed in ASRCu compared to ASR, with no apparent correlation between the enhancement and residue proximity to the paramagnetic center, which in this case is attached to C148 in the E–F loop on the cytoplasmic side. For example, we see that signals from residues A55, I56, and D57, at the extracellular flank of helix B and in the BC loop on the extracellular side, are as strong as those from F172 and T173, located in the middle of helix F close to the CuEDTA label. Thus, evaluation of the relative signal-to-noise ratio values obtained for resolved peaks shows that there is moderate, yet fairly uniform, enhancement across the entire protein in ASRCu, despite the paramagnetic probe having access only to the specific site in the EF loop of the protein.

With the addition of 40 mM CuEDTA we observe a significant overall increase in enhancement with an average value of 1.6 ± 0.3. Site-specific analysis shown in Fig. 4 suggests that the observed sensitivity enhancement is not homogeneous, and is larger in the loops (e.g., the BC loop) and in other solvent-accessible regions within helices, e.g., T170 (Shi et al. 2011; Wang et al. 2013). We also observe that signals from some transmembrane residues are only moderately enhanced (e.g., T79, T80, P81). Interestingly, helix C is well protected according to previously published hydrogen/deuterium exchange data (Shi et al. 2011; Wang et al. 2013), suggesting that the proximity to solvent exposed fragments and possible CuEDTA binding sites appears to be important. Overall, however, despite this variation of T_1 in the sample, it appears that spin diffusion is not a limiting factor in ASR, and is sufficient to transfer the ^{1}H spin–lattice PRE effect over the entire protein.

Due to the small decrease in the bulk ^{1}H T_1 values between ASR40Cu and ASR80Cu and the generally low signal to noise ratio of peaks, we did not expect to observe much greater enhancement in ASR80Cu when compared to ASR40Cu. Indeed, as shown in Fig. 4, signals from most

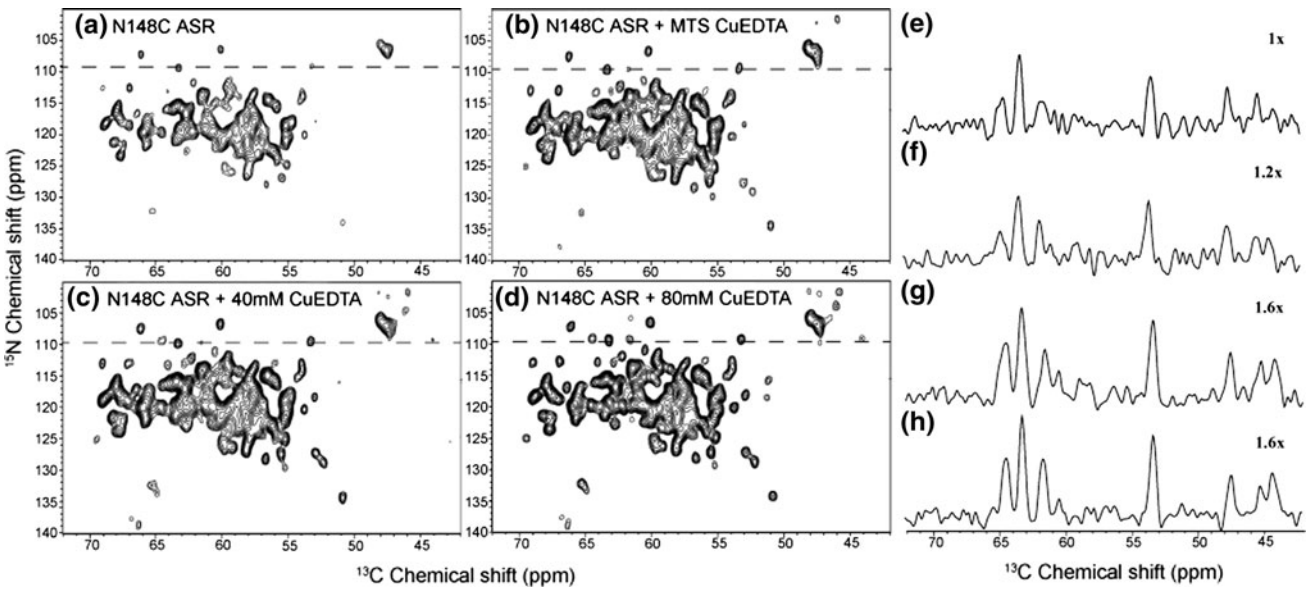

Fig. 3 2D NCA spectra of diamagnetic ASR (**a**), ASRCu (**b**), ASR40Cu (**c**), and ASR80Cu (**d**). All spectra were collected at a spinning frequency of 50 kHz and with the same total acquisition time, but with different recycle delays D_1 and number of scans NS: In **a** $D_1 = 450$ ms, NS = 792; **b** $D_1 = 295$ ms, NS = 1,208; **c** $D_1 = 150$ ms, NS = 1,920; **d** $D_1 = 135$ ms, NS = 2,064. Note that the length of the pulse sequence and acquisition, ~40 ms, contributes non-negligibly to the total experimental time in experiments with short D_1. All data sets were processed identically using Lorentzian-to-Gaussian apodization in both dimensions. For each spectrum the lowest contour level is cut at $7 \times \sigma$. **e–h** 1D traces extracted from 2D spectra of ASR (**e**), ASRCu (**f**), ASR40Cu (**g**), and ASR80Cu (**h**) at the positions indicated by *dashed lines* with scaling factors indicated

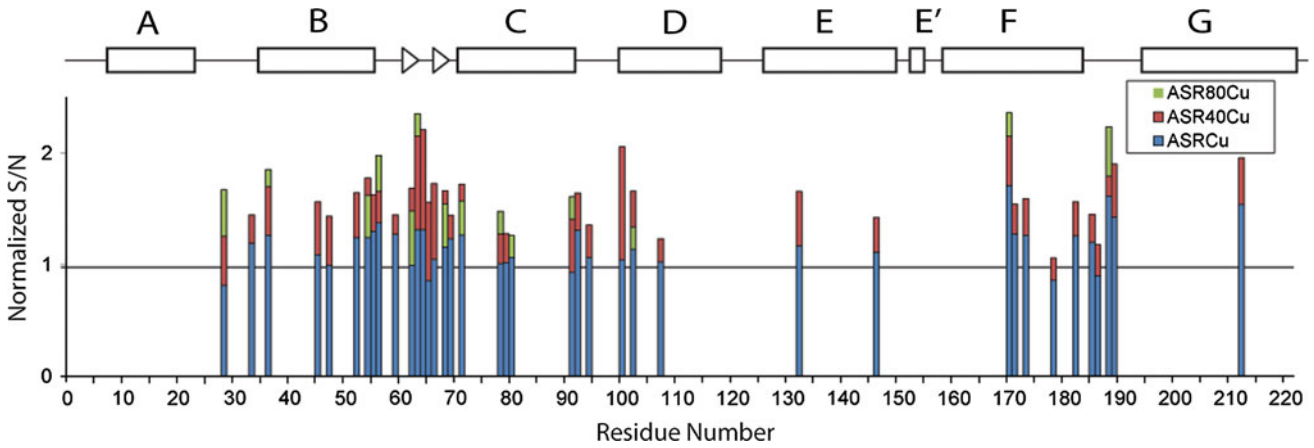

Fig. 4 Site-specific comparison of the relative S/N of ASRCu (*blue*), ASR40Cu (*red*), and ASR80Cu (*green*) for residues which are resolved in all four 2D NCA spectra. All S/N values are normalized to those in spectra of diamagnetic ASR considering the same sample quantities and experimental time. The secondary structure of ASR derived from solid-state NMR studies (Wang et al. 2013) is shown on *top*. In cases where sensitivity enhancement is not significantly different between ASR40Cu and ASR80Cu, no ASR80Cu *bar* is shown

residues have similar signal-to-noise ratios in the two spectra, and the average increase in enhancement in ASR80Cu is also 1.6 ± 0.3. There are, however, several residues, primarily in the exposed regions, which experience a larger than average sensitivity increase in ASR80Cu, which may be attributed to more even distribution of the paramagnetic enhancers on the protein surface.

It is instructive to directly compare the ^{13}C-detected experiments performed on the 1.3 mm probe at 50 kHz MAS with those which we obtain on a fully packed rotor in a Bruker 3.2 mm E-free probe with high power decoupling at moderate spinning rates (14–15 kHz), and with a typical recycle delay of 1.7 s. Although under optimal conditions on the 1.3 mm probe (ASR40Cu or ASR80Cu) the recycle delay can be reduced by a factor of approximately 13, we still see approximately a 3× sensitivity decrease. The sensitivity per unit mass is however greatly increased (∼5×). These results are summarized in Table 2. Thus, in situations when a protein can be expressed in sufficient quantities, the 3.2 mm probe is a better choice, as it provides better overall ^{13}C sensitivity. For mass-limited samples of proteins of 27 kDa investigated in this study, the sensitivity obtained using 1.3 mm probe is sufficient for applications involving 2D spectroscopy, but unlikely to be adequate for more complex 3D applications.

Table 2 Sensitivity comparison between the 3.2 mm EFREE probe and the 1.3 mm probe under optimized PACC conditions

Probe	^{13}C-detected experiments		^{1}H-detected experiments	
	3.2 mm	1.3 mm	3.2 mm	1.3 mm
Spinning frequency (kHz)	14.3	50	20.5	50
Relative volume	1	∼0.067	1	∼0.067
Recycle delay (s)	1.7	0.135	3	0.250
Relative sensitivity/scan[a]	1	∼0.11	1	∼0.4
Relative sensitivity/unit time[b]	1	∼0.33	1	∼1
Relative sensitivity/unit sample[c]	1	∼5	1	∼15

[a] Relative sensitivity of a single scan with a recycle delay of at least 3*T_1

[b] Relative sensitivity measured over a constant time

[c] Sensitivity per unit sample measured over a constant time

Paramagnetically enhanced proton-detected experiments

To investigate the potential of the PACC scheme for proton-detected spectroscopy of membrane proteins, we created two uniformly ^{2}H,^{13}C,^{15}N-labeled samples of PR. One sample was prepared without CuEDTA as a control (DPR), and one with 80 mM CuEDTA (DPR80Cu). Both samples contained 40 % H_2O in the solvent. The ^{1}H T_1 of DPR was measured to be 460 ms, and with the addition of 80 mM CuEDTA this value was reduced to 189 ms. The longer T_1 values than those measured on UCN N148C ASR are likely due to the fact that the proton bath is severely diminished by deuteration, resulting in less efficient spin diffusion between protons, as has been observed previously in α-spectrin SH3 domain (Linser et al. 2007).

To further investigate the effect of CuEDTA on our deuterated samples we collected 2D ^{1}H-^{15}N heteronuclear correlation spectra on both samples. In Fig. 5, we compare these spectra with that obtained using a 3.2 mm TL2 Bruker probe at a spinning rate of 20.5 kHz.

Taking advantage of the relatively short proton T_1, faster recycling can be used even in diamagnetic samples. Remarkably, despite a ~15-fold reduction in the amount of sample packed in 1.3 mm rotor, it took only 80 min to collect a 2D ^{1}H-^{15}N correlation spectrum with sensitivity similar to that from a 3.2 mm rotor (Fig. 5a, b). We have previously established that the proton line width in PR is dominated by inhomogeneous contributions (Ward et al. 2011). In accordance, although the bulk coherence life time, T_2', is strongly dependent on the spinning rate—we determined a value of 4.4 ms at 50 kHz, compared to 2.4 ms at 20.5 kHz (Ward et al. 2011)—the proton line widths are the same, on the order of 0.15–0.25 ppm in both spectra.

The addition of 80 mM CuEDTA leads to a fairly uniform apparent reduction of ^{1}H T_1, which allows for faster experimental recycling, allowing spectra of similar sensitivity to be collected in 35 min. However, CuEDTA appears to induce some spectral changes. The most obvious one is the disappearance of several peaks in the spectrum in Fig. 5c, namely the side chain signals of Q183 and N176, located in the E–F loop on the cytoplasmic side, which may be due to CuEDTA binding. Although to a much lesser extent, the intensity of G169, which is found in the same E–F loop, is also diminished, as can be seen in Fig. 5. Apart from these differences the rest of the spectra are of similar intensity to that of diamagnetic PR in Fig. 5b.

Proton detection is found to display an even better increase in efficiency than carbon detection. As summarized in Table 2, initial investigations of the sensitivity show that the experiments performed on the 1.3 mm probe have only ~2.5× lower sensitivity than those collected on the 3.2 mm probe. As recycle delays during proton-detected experiments on the 3.2 mm probe are increased due to decoupling applied to the nitrogen channel during acquisition ($D_1 \approx 3$ s), despite the reduced enhancement of ^{1}H T_1 relaxation times, caused by the extensive deuteration of the sample, we are still able to recycle proton detected experiments 12× faster on the 1.3 mm probe. Therefore the 1.3 mm probe and the 3.2 mm probe can achieve comparable sensitivities in a given time. In proteins with higher structural homogeneity than PR, proton detection would further benefit from faster MAS rates, resulting in higher spectral resolution and sensitivity (Lewandowski et al. 2011). Thus, the development of proton-detected experiments for characterizing membrane proteins in the 1.3 mm probe would be beneficial, as the characterization of a protein would then require only ~1/15 of the sample required for the 3.2 mm probe, and still obtain the same

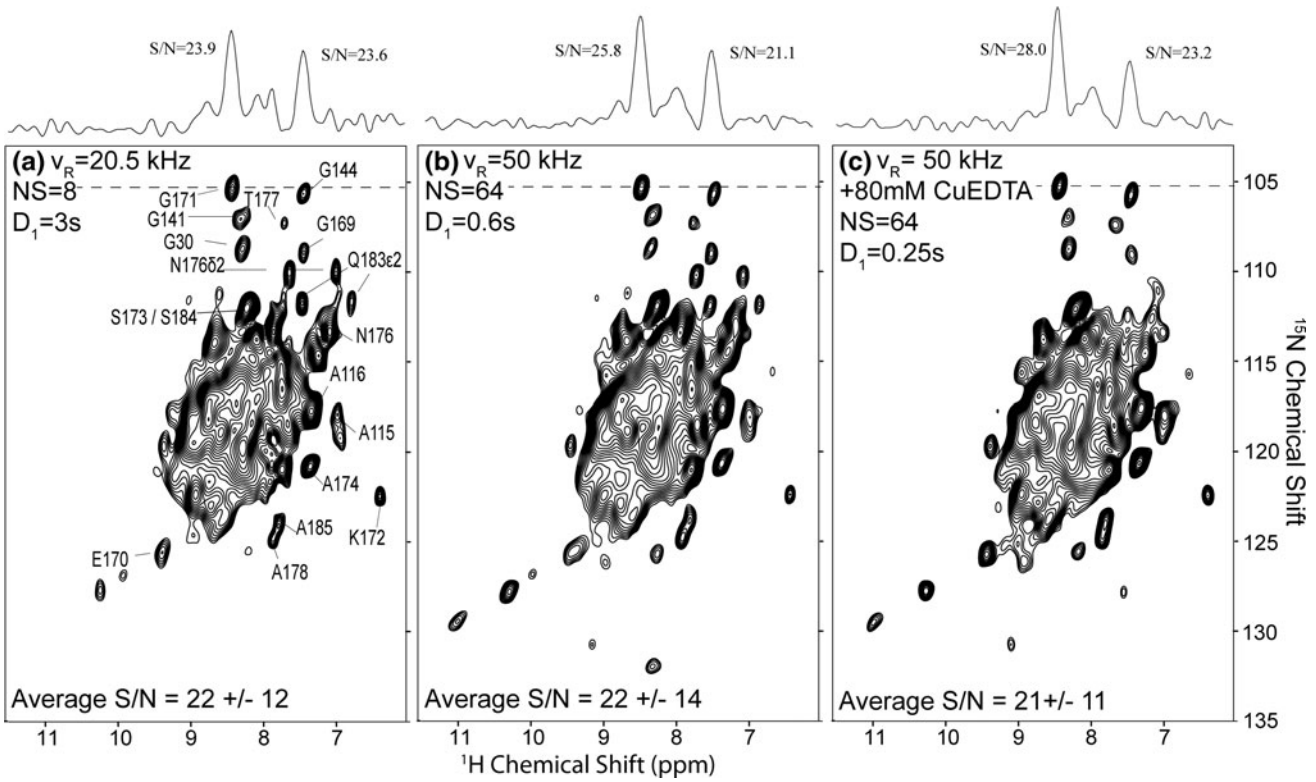

Fig. 5 ^{1}H-^{15}N heteronuclear correlation spectra of U-[^{2}H-^{15}N-^{13}C]-PR. Diamagnetic PR at a spinning frequency of 20.5 kHz (**a**), 50 kHz (**b**), and (**c**) 50 kHz with 80 mM CuEDTA added to the solvent. In all cases exchangeable sites are protonated at 40 %. *Dashed lines* indicate the position of the slices shown above the spectra. Experimental times were 45, 80, and 35 min respectively. The lowest contour on each spectrum is cut at 10 × σ. S/N values for individual peaks are noted beside 1D slices

sensitivity, either in protonated or per-deuterated samples in cases when such samples can be produced.

Conclusions

We have investigated the utility of the previously introduced paramagnetic relaxation-assisted condensed data collection (PACC) scheme for applications to relatively large 7TM proteins packed in a small 1.3 mm rotor. Between the two studied paramagnetic doping schemes, the covalent introduction of CuEDTA in one of the loops, and the addition of CuEDTA in solution, the latter provided much better paramagnetic relaxation enhancements and, in combination with low power decoupling and magic angle spinning of 50 kHz, permitted fast recycle delays of 135 ms ($1.3T_1$) in samples containing 80 mM CuEDTA (approximately 8 Cu^{2+} ions per ASR molecule). This is approximately 13 times faster compared to traditional methods used in larger 3.2 mm probes. However, due to the small sample volume the overall sensitivity per unit time in carbon-detected experiments was still lower than that seen in the 3.2 mm probe.

In contrast, the sensitivity of proton detection in a 1.3 mm probe is comparable to that observed earlier in the TL2 Bruker 3.2 mm probe (Ward et al. 2011). Furthermore, the 1.3 mm probe offers the benefit of faster spinning rates, which in samples with homogeneous proton line widths provides additional sensitivity enhancements (Lewandowski et al. 2011). This is an attractive prospect for studies of samples that can only be produced in limited quantity.

Acknowledgments This research was supported by the Natural Sciences and Engineering Research Council of Canada (Discovery Grants to V. L. and L. S. B.), the Canada Foundation for Innovation, and the Ontario Ministry of Economic Development and Innovation. V. L. holds a Canada Research Chair in Biophysics. M. W. is a recipient of an NSERC PGS fellowship. We thank So Young Kim and Kwang-Hwan Jung (Sogang University, Seoul, Korea) for the generous gift of a plasmid encoding N148C ASR.

References

Asami S, Szekely K, Schanda P, Meier BH, Reif B (2012) Optimal degree of protonation for ^{1}H detection of aliphatic sites in randomly deuterated proteins as a function of the MAS frequency. J Biomol NMR 54:155–168. doi:10.1007/s10858-012-9659-9

Baldus M, Petkova AT, Herzfeld J, Griffin RG (1998) Cross polarization in the tilted frame: assignment and spectral simplification in heteronuclear spin systems. Mol Phys 95:1197–1207

Bertini I, Luchinat C, Parigi G (2001) Solution NMR of paramagnetic molecules: applications to metallobiomolecules and models. In: Current methods in inorganic chemistry, vol. 2. Elsevier, Amsterdam, pp. 1–372

Cady SD, Schmidt-Rohr K, Wang J, Soto CS, Degrado WF, Hong M (2010) Structure of the amantadine binding site of influenza M2 proton channels in lipid bilayers. Nature 463:689–692. doi:10.1038/nature08722

Delaglio F, Grzesiek S, Vuister GW, Zhu G, Pfeifer J, Bax A (1995) NMRPipe: a multidimensional spectral processing system based on UNIX pipes. J Biomol NMR 6:277–293

Egorova-Zachernyuk TA, Bosman GJCGM, Degrip WJ, Shvets VI (2010) Stable isotope labelling of human histamine receptor H1R: prospects for structure-based drug design. Dokl Biochem Biophys 433:164–167. doi:10.1134/S160767291004006X

Egorova-Zachernyuk TA, Bosman GJCGM, Degrip WJ (2011) Uniform stable-isotope labeling in mammalian cells: formulation of a cost-effective culture medium. Appl Microbiol Biotechnol 89:397–406. doi:10.1007/s00253-010-2896-5

Ernst M, Meier MA, Tuherm T, Samoson A, Meier BH (2004) Low-power high-resolution solid-state NMR of peptides and proteins. J Am Chem Soc 126:4764–4765. doi:10.1021/ja0494510

Friedrich T, Geibel S, Kalmbach R, Chizhov I, Ataka K, Heberle J, Engelhard M, Bamberg E (2002) Proteorhodopsin is a light driven proton pump with variable vectoriality. J Mol Biol 321:821–838. doi:10.1016/s0022283602006964

Hartmann SR, Hahn EL (1962) Nuclear double resonance in the rotating frame. Phys Rev 128:2042–2053

Hong M (2007) Structure, topology, and dynamics of membrane peptides and proteins from solid-state NMR spectroscopy. J Phys Chem B 111:10340–10351. doi:10.1021/jp073652j

Hu F, Luo W, Hong M (2010) Mechanisms of proton conduction and gating in influenza M2 proton channels from solid-state NMR. Science 330:505–508. doi:10.1126/science.1191714

Jaroniec CP (2012) Solid-state nuclear magnetic resonance structural studies of proteins using paramagnetic probes. Solid State Nucl Magn Reson 43–44:1–13. doi:10.1016/j.ssnmr.2012.02.007

Jung KH, Trivedi VD, Spudich JL (2003) Demonstration of a sensory rhodopsin in eubacteria. Mol Microbiol 47:1513–1522

Kano K, Fendler JH (1978) Pyranine as a sensitive pH probe for liposome interiors and surfaces. Biochim Biophys Acta 509:289–299

Keller R (2004) The computer aided resonance assignment tutorial, 1st edn. Goldau, Switzerland

Kotecha M, Wickramasinghe NP, Ishii Y (2007) Efficient low-power heteronuclear decoupling in 13C high-resolution solid-state NMR under fast magic angle spinning. Magn Reson Chem 45(Suppl 1):S221–S230. doi:10.1002/mrc.2151

Lewandowski JR, Sein J, Sass HJ, Grzesiek S, Blackledge M, Emsley L (2010) Measurement of site-specific 13C spin-lattice relaxation in a crystalline protein. J Am Chem Soc 132:8252–8254. doi:10.1021/ja102744b

Lewandowski JR, Dumez J, Akbey Ü, Lange S, Emsley L, Oschkinat H (2011) Enhanced resolution and coherence lifetimes in the solid-state NMR spectroscopy of perdeuterated proteins under ultrafast magic-angle spinning. J Phys Chem Lett 2:2205–2211

Linser R, Chevelkov V, Diehl A, Reif B (2007) Sensitivity enhancement using paramagnetic relaxation in MAS solid-state NMR of perdeuterated proteins. J Magn Reson 189:209–216. doi:10.1016/j.jmr.2007.09.007

Marchetti A, Jehle S, Felletti M, Knight MJ, Wang Y, Xu Z-Q, Park AY, Otting G, Lesage A, Emsley L, Dixon NE, Pintacuda G (2012) Backbone assignment of fully protonated solid proteins by 1H detection and ultrafast magic-angle-spinning NMR spectroscopy. Angew Chem Int Ed Engl 51:10756–10759. doi:10.1002/anie.201203124

Marion D, Wüthrich K (1983) Application of phase sensitive two-dimensional correlated spectroscopy (COSY) for measurements of 1H-1H spin–spin coupling constants in proteins. Biochem Biophys Res Commun 113:967–974

Markley JL (1971) Spin-lattice relaxation measurements in slowly relaxing complex spectra. J Chem Phys 55:3604. doi:10.1063/1.1676626

McDermott A (2009) Structure and dynamics of membrane proteins by magic angle spinning solid-state NMR. Annu Rev Biophys 38:385–403. doi:10.1146/annurev.biophys.050708.133719

Morcombe CR, Zilm KW (2003) Chemical shift referencing in MAS solid state NMR. J Magn Reson 162:479–486

Nadaud PS, Helmus JJ, Sengupta I, Jaroniec CP (2010) Rapid acquisition of multidimensional solid-state NMR spectra of proteins facilitated by covalently bound paramagnetic tags. J Am Chem Soc 132:9561–9563. doi:10.1021/ja103545e

Naito A (2009) Structure elucidation of membrane-associated peptides and proteins in oriented bilayers by solid-state NMR spectroscopy. Solid State Nucl Magn Reson 36:67–76. doi:10.1016/j.ssnmr.2009.06.008

Nishiyama Y, Endo Y, Nemoto T, Utsumi H, Yamauchi K, Hioka K, Asakura T (2011) Very fast magic angle spinning (1)H-(14)N 2D solid-state NMR: sub-micro-liter sample data collection in a few minutes. J Magn Reson 208:44–48. doi:10.1016/j.jmr.2010.10.001

Park SH, Das BB, Casagrande F, Tian Y, Nothnagel HJ, Chu M, Kiefer H, Maier K, De Angelis AA, Marassi FM, Opella SJ (2012) Structure of the chemokine receptor CXCR1 in phospholipid bilayers. Nature 491:779–783. doi:10.1038/nature11580

Pines A, Gibby MG, Waugh JS (1973) Proton-enhanced NMR of dilute spins in solids. J Chem Phys 59:569–590

Ramamoorthy A (2009) Beyond NMR spectra of antimicrobial peptides: dynamical images at atomic resolution and functional insights. Solid State Nucl Magn Reson 35:201–207. doi:10.1016/j.ssnmr.2009.03.003

Religa TL, Ruschak AM, Rosenzweig R, Kay LE (2011) Site-directed methyl group labeling as an NMR probe of structure and dynamics in supramolecular protein systems: applications to the proteasome and to the ClpP protease. J Am Chem Soc 133:9063–9068. doi:10.1021/ja202259a

Renault M, Cukkemane A, Baldus M (2010) Solid-state NMR spectroscopy on complex biomolecules. Angew Chem Int Ed Engl 49:8346–8357. doi:10.1002/anie.201002823

Schanda P, Meier BH, Ernst M (2010) Quantitative analysis of protein backbone dynamics in microcrystalline ubiquitin by solid-state NMR spectroscopy. J Am Chem Soc 132:15957–15967. doi:10.1021/ja100726a

Sengupta I, Nadaud PS, Helmus JJ, Schwieters CD, Jaroniec CP (2012) Protein fold determined by paramagnetic magic-angle spinning solid-state NMR spectroscopy. Nat Chem 4:410–417. doi:10.1038/nchem.1299

Shahid SA, Bardiaux B, Franks WT, Krabben L, Habeck M, van Rossum B-J, Linke D (2012) Membrane-protein structure determination by solid-state NMR spectroscopy of microcrystals. Nat Methods 9:1212–1217. doi:10.1038/nmeth.2248

Shaka AJ, Keeler J, Freeman R (1983) Evaluation of a new broadband decoupling sequence: WALTZ-16. J Magn Reson 53:313–340

Sharma M, Yi M, Dong H, Qin H, Peterson E, Busath DD, Zhou H-X, Cross TA (2010) Insight into the mechanism of the influenza a proton channel from a structure in a lipid bilayer. Science 330:509–512. doi:10.1126/science.1191750

Shi L, Yoon SR, Bezerra AG, Jung K-H, Brown LS (2006) Cytoplasmic shuttling of protons in Anabaena sensory rhodopsin: implications for signaling mechanism. J Mol Biol 358:686–700. doi:10.1016/j.jmb.2006.02.036

Shi L, Ahmed MA, Zhang W, Whited G, Brown LS, Ladizhansky V (2009a) Three-dimensional solid-state NMR study of seven-helical integral membrane proton pump–structural insights. J Mol Biol 386:1078–1093

Shi L, Lake EMR, Ahmed MAM, Brown LS, Ladizhansky V (2009b) Solid-state NMR study of proteorhodopsin in the lipid environment: secondary structure and dynamics. Biochim Biophys Acta 1788:2563–2574. doi:10.1016/j.bbamem.2009.09.011

Shi L, Kawamura I, Jung K-H, Brown LS, Ladizhansky V (2011) Conformation of a seven-helical transmembrane photosensor in the lipid environment. Angew Chem Int Ed 50:1302–1305. doi:10.1002/anie.201004422

Tang M, Berthold DA, Rienstra CM (2011) Solid-state NMR of a large membrane protein by paramagnetic relaxation enhancement. J Phys Chem Lett 2:1836–1841. doi:10.1021/jz200768r

Thurber KR, Tycko R (2009) Measurement of sample temperatures under magic-angle spinning from the chemical shift and spin-lattice relaxation rate of 79Br in KBr powder. J Magn Reson 196:84–87. doi:10.1016/j.jmr.2008.09.019

Vijayan V, Demers J-P, Biernat J, Mandelkow E, Becker S, Lange A (2009) Low-power solid-state NMR experiments for resonance assignment under fast magic-angle spinning. ChemPhysChem 10:2205–2208. doi:10.1002/cphc.200900439

Wada Y, Kawanabe A, Furutani Y, Kandori H, Ohtani H (2008) Quantum yields for the light adaptations in Anabaena sensory rhodopsin and bacteriorhodopsin. Chem Phys Lett 453:105–108. doi:10.1016/j.cplett.2008.01.010

Wang S, Munro R, Kim S, Jung K-H, Brown LS, Ladizhansky V (2012) Paramagnetic relaxation enhancement reveals oligomerization interface of a membrane protein. J Am Chem Soc 134:16995–16998

Wang S, Munro RA, Shi L, Kawamura I, Okitsu T, Wada A, Kim S-Y, Jung K-H, Brown LS, Ladizhansky V (2013) Solid-state NMR spectroscopy structure determination of a lipid-embedded heptahelical membrane protein. Nat Methods 10:1007–1015. doi:10.1038/nmeth.2635

Ward M, Shi L, Lake EM, Krishnamurthy S, Hutchins H, Brown LS, Ladizhansky V (2011) Proton-detected solid-state NMR reveals intermembrane polar networks in a seven-helical transmembrane protein proteorhodopsin. J Am Chem Soc 133:17434–17443

Werner K, Richter C, Klein-Seetharaman J, Schwalbe H (2008) Isotope labeling of mammalian GPCRs in HEK293 cells and characterization of the C-terminus of bovine rhodopsin by high resolution liquid NMR spectroscopy. J Biomol NMR 40:49–53. doi:10.1007/s10858-007-9205-3

Wickramasinghe NP, Kotecha M, Samoson A, Past J, Ishii Y (2007) Sensitivity enhancement in (13)C solid-state NMR of protein microcrystals by use of paramagnetic metal ions for optimizing (1)H T(1) relaxation. J Magn Reson 184:350–356. doi:10.1016/j.jmr.2006.10.012

Wickramasinghe NP, Parthasarathy S, Jones CR, Long F, Kotecha M, Mehboob S, Fung LW, Samoson A, Ishii Y (2009) Nanomole-scale protein solid-state NMR by breaking intrinsic 1H-T1 boundaries. Nat Methods 6:215–218. doi:10.1038/nmeth.1300

Yamamoto K, Xu J, Kawulka KE, Vederas JC, Ramamoorthy A (2010) Use of a copper-chelated lipid speeds up NMR measurements from membrane proteins. J Am Chem Soc 132:6929–6931. doi:10.1021/ja102103n

Zhou DH, Shah G, Cormos M, Mullen C, Sandoz D, Rienstra CM (2007) Proton-detected solid-state NMR spectroscopy of fully protonated proteins at 40 kHz magic-angle spinning. J Am Chem Soc 129:11791–11801. doi:10.1021/ja073462m